11.5 VARIABILITY AND VERTICAL STRUCTURE OF THE SUMMER ARCTIC BOUNDARY LAYER

Michael Tjernström and Thorsten Mauritsen
Stockholm University, Stockholm, Sweden

1. INTRODUCTION

The Arctic is expected to experience an amplified warming due to global anthropogenic climate change. In an ensemble of 19 CMIP (Coupled Model Intercomparison Project, Meehl et al., 2000) simulations, the Arctic is expected to warm at about 2.5 times the global average (Räisenen 2001). However, the inter-model differences in are larger in the Arctic than elsewhere on Earth, ranging from an amplification factor of 1.5 to 5 (Räisenen 2001). At the same time, the many of the global models used for these estimates have difficulties in simulating even the present climate (Walsh et al. 2002). This uncertainty in Arctic climate sensitivity arises to a large extent from an insufficient understanding of several strong feedback processes, that often need to be parameterized.

Model studies in the Arctic Climate Model Intercomparison project (ARCMIP, Curry and Lynch, 2002) suggest that much of the problems reside in the boundary layer (Tjernström et al. 2004). Development of parameterizations will always remain empirical to some extent. New schemes are based partly on and are evaluated against field experiment data on important processes. This poses a special problem in the Arctic, since the amount of field experiment data remains limited. This paper deals with the boundary-layer vertical structure and variability analyzed from data taken during the Arctic Ocean 2001 (AOE-2001) experiment.

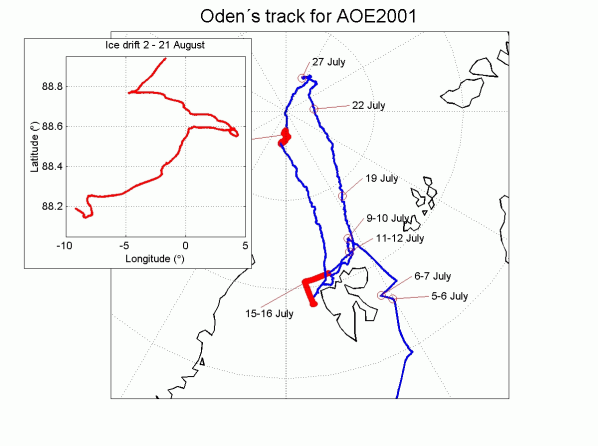

Figure 1. Cruise track (blue) of the AOE-2001 expedition with research stations with dates marked in red. The ice drift is shown in the insert.

2. THE EXPERIMENT

A main goal of the AOE-2001 expedition during summer 2001 was to study the summer high-Arctic boundary layer, in particular the physical and chemical mechanisms behind the formation of aerosols and boundary-layer clouds. AOE-2001 was based on the Swedish icebreaker *Oden*. A primary focus on a three-week ice drift 88-89 ºN, around 0 ºE in August 2001[1].

Figure 1 shows the expedition cruise track; the insert shows the ice drift in detail. During this main phase of the expedition, the icebreaker was moored to a 1.5 x 3 km^2 large ice floe (Figure 2). Remote sensing instrumentation (a wind profiler, a cloud/precipitation radar and a passive scanning infrared radiometer) remained onboard, while two sodar systems were deployed on the ice. Also onboard was a weather station continuously logging regular weather information, including a laser cellometer cloud base and visibility from a backscatter instrument. Soundings were also released onboard. Additionally on the ice, an 18-m profile and turbulence mast was deployed and two Integrated Surface Flux Facility stations were also deployed, on nearby ice floes. Tjernström et al. (2004) gives a detailed account of the measurement program.

3. THE SUMMER ARCTIC BOUNDARY-LAYER VERTICAL STRUCTURE

One inherent feature in the summer Arctic boundary layer, that needs to be considered, is the high concentration of low-level clouds. Ceilometer and cloud-radar data indicate that the summer boundary layer was cloud capped a significant portion of the time, > 95 %, (Tjernström 2004). Cloud systems were occasionally associated with synoptic weather systems, but most of the time they were boundary-layer clouds, most commonly with a lowest cloud base around or below 100 m and cloud tops varying between 200 and 600 m. Under the stratus base, patchy fogs often occurred (Tjernström 2004).

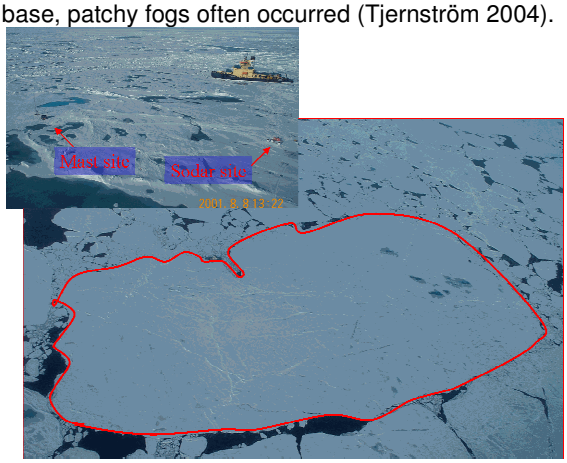

Figure 2. Photo of the ice floe used for the AOE-2001 ice drift. Insert shows two of the instrument sites in the foreground with the icebreaker *Oden* in the background. Note the small harbor on the upper edge of the floes, where *Oden* can be seen.

* ***Corresponding author address:*** **Michael Tjernström, Stockholm University, Department of Meteorology, SE-106 91 Stockholm, Sweden. Email:** michaelt@misu.su.se

[1] Throughout this text, “Julian Date” (JD) and “Day of the Year” (DOY) are used interchangeably, always meaning day after 1 January, with DOY=1.0 at 0000 UTC on 1 January.

The passive 5 mm scanning radiometer, deployed on *Oden*, is insensitive to weather conditions, and provided a record of vertical temperature profiles with a very high temporal resolution. The scanning period of the instrument is 0.4 sec; to reduce noise scans are averaged to ~ 5 min averages. The radiometer scans 360º in the vertical plane, and therefore its resolution successively degrades with altitude, to a top height around 1 km. During AOE-2001, the radiometer was constrained by the low-level air temperatures from the mast on the ice and by results from 6-hourly soundings. Figure 3 shows an example of a time-height cross-section of radiometer temperatures, along with some other data on clouds, precipitation and visibility, from other sensors.

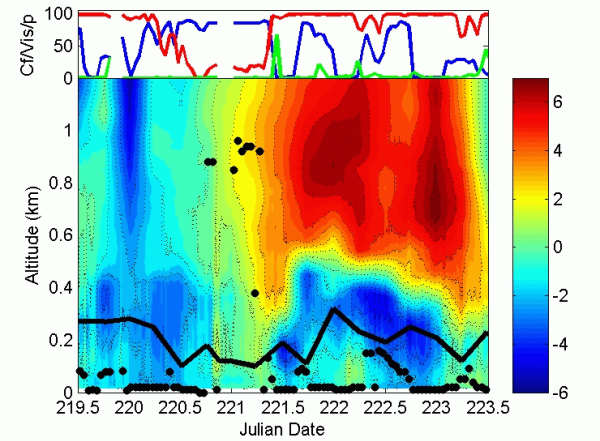

Figure 3. Time-height cross-section of radiometer temperature for a four-day period (time is in DOY). Overlaid are cloud base (solid dots) and PBL depth (solid line). In the top panel, red is cloud fraction (%), blue is visibility (km) and green is precipitation intensity (arbitrary units).

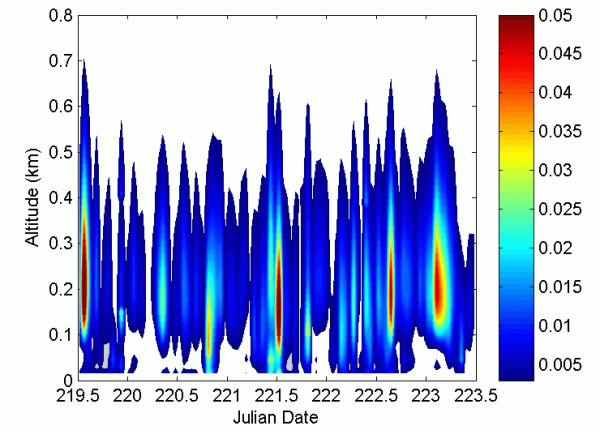

Figure 4. Time-height cross-section of profiles of 5 min to 1-hour band-pass filtered temperature variances for the episode in Figure 3.

The period shown as an example in Figure 3, includes the strongest warm-air advection episode during AOE-2001, and also one of the few longer periods with almost clear conditions, preceding the first warm front arriving just before DOY 221.5. The episode ends with the passage of a cold front around DOY 223.1. At both the major frontal passages, the radiometer temperatures indicate strong entrainment events, with warm free-troposphere air reaching almost all the way to the surface. In the warm air sector, the boundary layer appears to be relatively well mixed and capped by a very strong inversion, with temperatures immediately above the inversion reaching ~ 8 ºC at DOY 223.0. The high temporal resolution of the radiometer makes possible a determination of the variability in the temperature profile record. Figure 4 shows the 5 min-to-1h band-pass filtered temperature variance from the radiometer. Frontal passages shows up clearly, but there are also other periods with higher variability for example at DOY 219.6, 220.8 and 222.6.

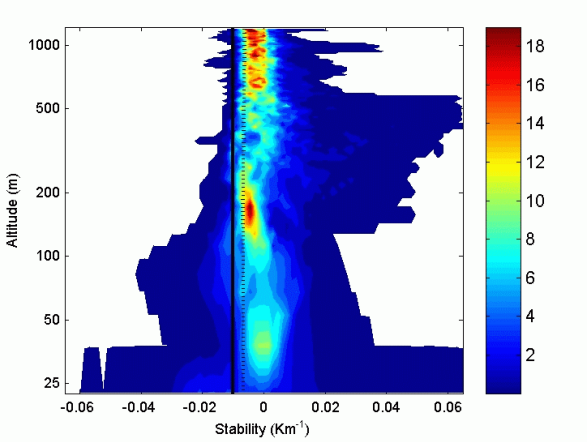

Figure 5. Contours of relative probability of the vertical temperature gradient, from an almost continuous record through the ice drift.

The high availability of this data throughout the experiment also makes a more general analysis possible. Figure 5 shows contours of relative probability of the vertical temperature gradient as a function of height, from the ice-drift. The near-surface temperature gradients tend to be mostly stable, with very few occasions of unstable stratification although it does occur. In an altitude range from ~ 100 m to 300-400 meter, the stability tends to mostly be close to moist adiabatic (dotted black line). This corresponds roughly to the most common layer of low-level clouds. It is topped by a stable, more variable layer up to ~ 500 m, corresponding to the capping inversion. Aloft, the lower free troposphere is stably stratified.

An objective analysis of the main capping and the surface inversions for the whole experiment are given in Figure 6. The surface inversions are here included also when they occur below a stronger capping inversion. The main inversions most often starts around ~ 200 m, and are anywhere between 200 and 600 deep. Surface inversions occur less frequently and are seldom deeper than 100 meters. The main inversion strength is most often 2 - 4 ºC, but inversions up to ~ 12 ºC occurs. The surface inversions are less strong, typically only < 2 ºC.

Boundary layer depths (Figure 7) were estimated from two sources. From the temperature and wind soundings, crude Richardson number profiles was calculated and the boundary-layer top was assigned to where this first became >1. Additionally, the height of the variance maximum in the radiometer temperature variance was used, assuming it to typically be located at the base of the

capping inversion. In a statistical sense, both boundary-layer depth estimates agree on a predominantly quite shallow boundary layer, most often ~ 150 m deep.

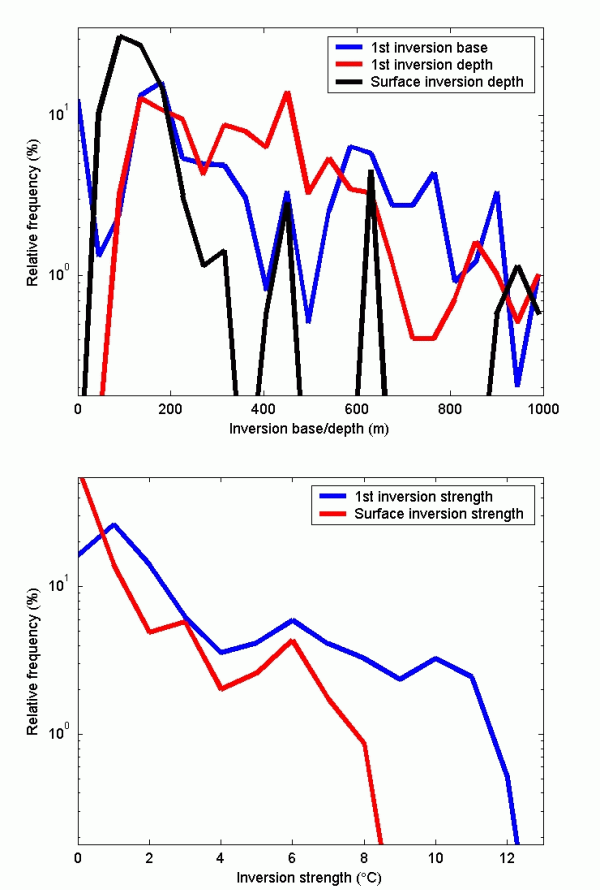

Figure 6. Statistics for inversion dimensions (top) and inversion strength (bottom) for the whole AOE-2001, from radiometer data.

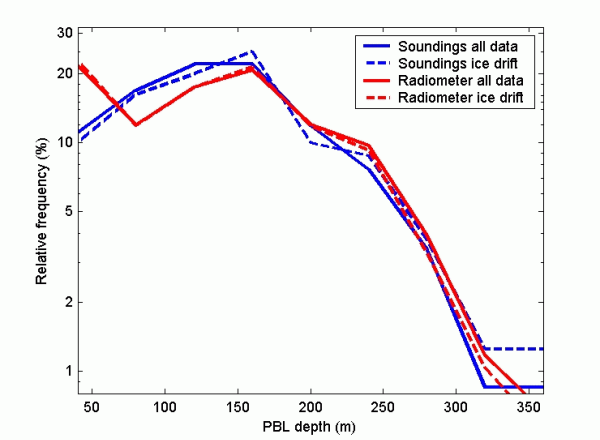

Figure 7. Statistics of boundary-layer depths derived from soundings and from radiometer temperature variance profiles.

The bulk boundary-layer stability was calculated from near-surface and inversion-base temperatures along with inversion base heights from the soundings. Its deviation from moist-adiabatic stratification (considering the very moist and often low-cloud capped boundary layer) was also calculated. This bulk stability is most often near moist-neutral, on the stable side (Figure 8).

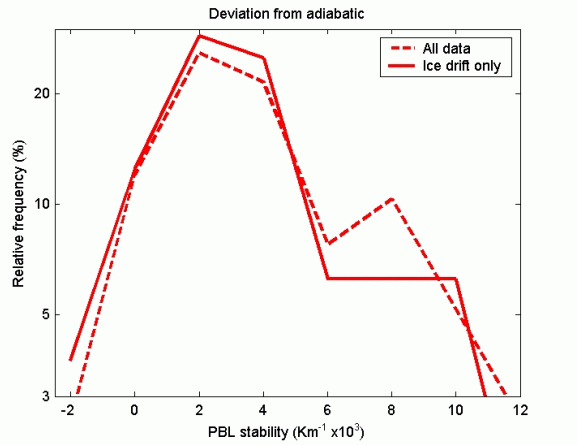

Figure 8. Bulk PBL stability from the radiometer record.

The picture that emerges is that of a shallow but relatively well-mixed and often cloudy boundary layer. The question arises what process facilitate to keep the boundary layer so well mixed. Surface friction certainly contributes in this shallow boundary layer, but cloud-top cooling should certainly also have been a factor had these observation been made in lower-latitude marine conditions. In that setting, the inversion base is expected to coincide with the cloud top, since that would be the location of the maximum cooling in a blackbody cloud.

This is, however, not always the case in the Arctic summer, as is borne out by Figure 9. This figure shows the relative frequency of occurrence of height differences between the cloud top, analyzed from cloud radar data, and the inversion base, taken from radiometer data. Although the cloud tops most commonly lies within 100 m from the inversion base, it is relatively common that the cloud top lies well within the inversion. A possible reason is that the blackbody assumption is not always valid in the summer Arctic (Garrett et al. 2002).

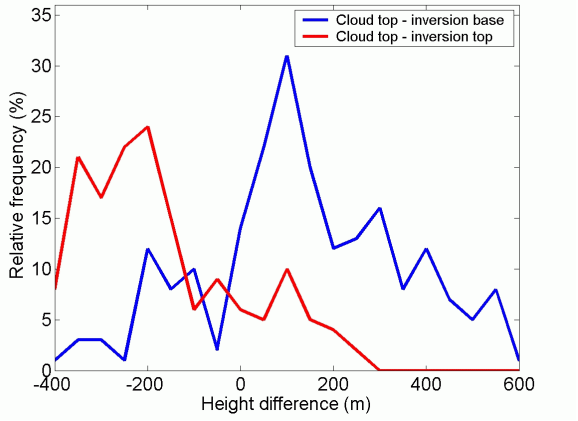

Figure 9. Statistics of cloud-top minus inversion base and inversion-top minus cloud-top distances, for the whole experiment.

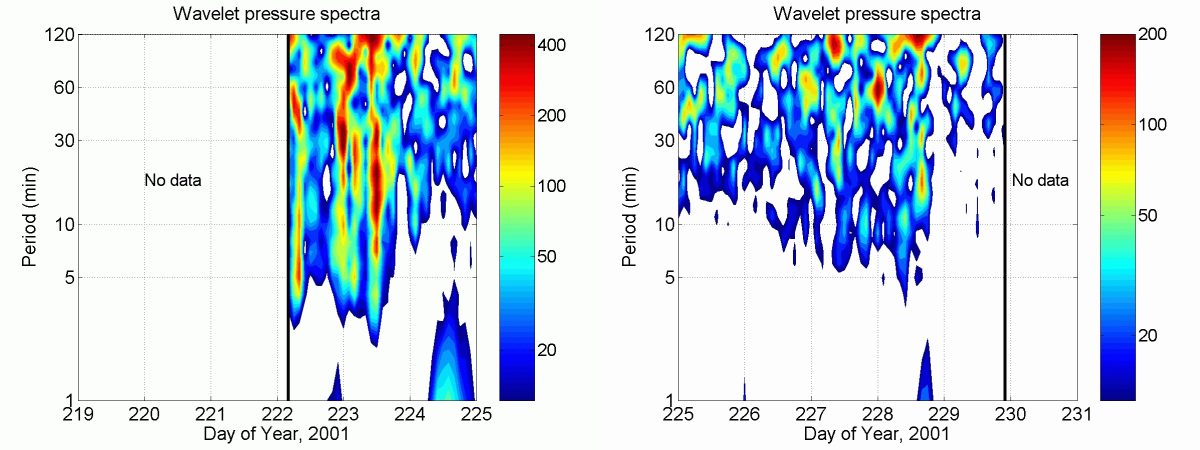

Figure 10. Contours of wavelet spectral amplitude of surface pressure, log ($p'*10^{-6}$), from one microbarograph sensor deployed on the ice. Note the change in scale between the left and right figure.

4. TEMPORAL VARIABILITY OF THE SUMMER ARCTIC BOUNDARY LAYER

One example of appreciable variability was seen already in Figure 4, showing the band-pass temperature variance. Some of this variability is off course related to the passage of frontal structures but on other occasions, other processes seem to be responsible. Rather than varying smoothly with time, high temperature variance occurs in bursts of enhanced magnitude.

Figure 10 also illustrates this kind of burst-like variability, in surface pressure from the wavelet spectral power of measurements from one microbarograph sensor. The record can be divided into four distinct periods. In the first, from the deployment until DOY ~ 224.2, there are several large-amplitude pressure variations starting at low frequency and at least on fours occasions cascading to higher frequency with periods of ~ 5 min. During the next period, DOY ~ 224.2 – 227, amplitudes are significantly lower and the bursts are fewer. This period starts with a peak in amplitude also at the very shortest periods – highest frequency. During the third period, DOY ~ 227 – 229, the amplitude increases again but only to a factor of two lower than during the first period or lower. In the last period, DOY > 229 until the end, surface pressure variability vanishes almost entirely.

During the first of these periods, some of strongest high-frequency events are related to frontal passages, but for example the event occurring around DOY 222.4 is from the period in the warm-sector air with a strong capping inversion and no frontal passages (Figure 3). In Figure 11, composite wind speed profiles from different instruments are shown, for the first period and from the transition between the first and second periods. Although there are discrepancies between different instruments, there are evidence of a low-level jet in time the period between the two main frontal passages, at ~ 200 – 400 m with the highest wind speeds reaching 7– 8 ms^{-1} at ~ 300 m. It seems possible that wave instabilities could be triggered in such conditions. Moreover, the transition to the second period with significantly lower activity, is marked by a significant increase in free-troposphere

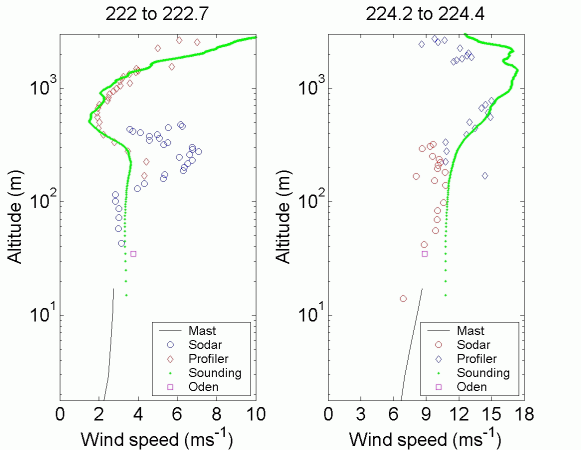

Figure 11. Composite wind speed profiles from different instruments (see the figure legend) for two time-periods.

wind speed, reaching 15 – 18 ms^{-1} at 1 – 3 km, erasing the jet-structure. This comes after the arrival of a series of cold fronts and the increase in high-frequency variability in the microbarograph pressure during this time may be due to increased turbulence intensity, due to the arrival of colder air over the almost constantly 0 - 2 ºC surface, enhancing buoyancy-generated turbulence; the increased wind speed may also have contributed.

Other evidence of low-frequency variability is found in the shape of the wind-speed power spectra from measurements on the main mast. From these, in particular for the across-wind component, three main types of spectral shapes were found, occurring consistently in time (Figure 12). During periods of sustained moderate to high turbulence, the spectral shape for some periods had the classical shape with a turbulent peak and a roll-off in spectral density at low frequencies. During other periods there was a pronounced spectral gap separating the turbulent peak from higher variability at lower frequency. Additionally, when the turbulence was weak, there were prolonged periods with almost no turbulence contribution to the spectral density and where variability at the lower frequencies dominated.

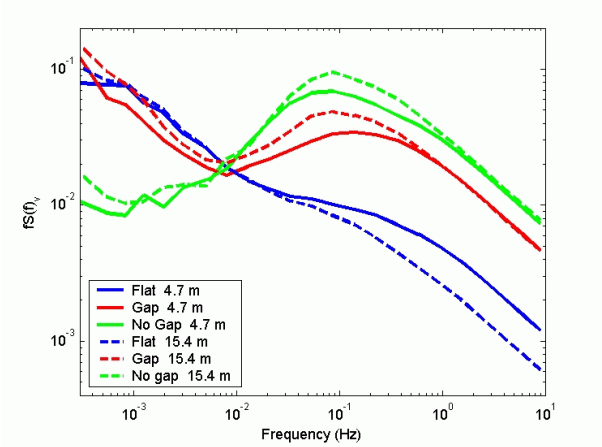

Figure 12. Averaged 1-h power spectra of differently classified across-wind wind-speed component for two heights in the main mast.

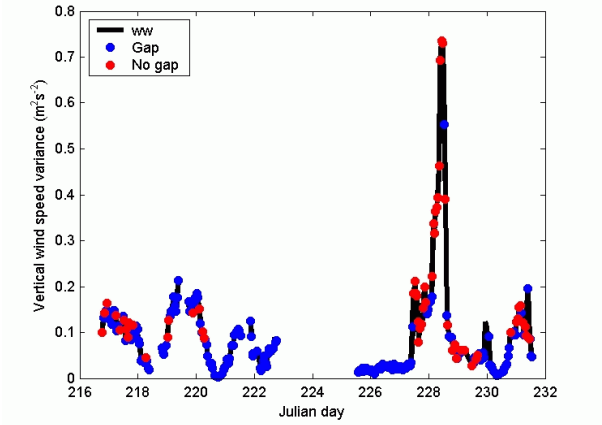

Figure 13. Time series of vertical velocity variance from the whole ice drift, with markers according to the legend indicating periods of different spectral shape.

Figure 12 shows the mean of all 1-hour across-wind spectra, classified objectively into those with a well-defined gap (22 %), those entirely without a gap (18 %) and those with only low-frequency variance (26 %), leaving 34 % of the sensor time unclassified. In Figure 13, the time-series of turbulence is illustrated, indicating periods of gap or no-gap conditions. It is clear that long periods of conditions with spectral gaps are interrupted by shorter periods without any gap. Unfortunately, there are almost no turbulence observations available for the DOY ~ 222 – 224 period, due to a computer failure. A somewhat similar period occurs during the period 227 – 229, however, then the remotes sensing winds are less good and winds aloft are uncertain. There are however indications that there was a low-level wind-speed maximum on top of the boundary layer also during this period.

5. DISCUSSION

The summer 2001 Artic boundary layer was shallow and capped by low-level clouds. A passive scanning 5 mm radiometer provides observations of the vertical thermal structure at a temporal resolution unprecedented in the Arctic. Stability mostly remained close to moist adiabatic, capped by an inversion that was sometimes very strong. Relatively often, however, cloud tops seemed to lie well into the inversion, rather than at the inversion base. This is an indication that the cloud emissivity may have been reduced, possibly by the lack of cloud condensation nuclei (CCN) causing clouds with few but large droplets (Garrett et al. 2002) in this very clean air.

Several types of instruments indicate frequently occurring low-frequency variability in the boundary layer. Such variations are evident in temperature variance from the radiometer, occurring in bursts rather than continuously, in the microbarograph record and in power spectra of surface-layer winds. Occasionally, the mean meteorology seems to be favorable for shear instability waves but more analysis will be necessary. Interesting to note is that there is a tendency for the capping-inversion Richardson number to be smaller when surface-layer spectra have a larger low-frequency contribution to the wind-speed variance.

More analysis will be required to find the source of the low-frequency variations in the boundary layer. It is also interesting to note, however, that although the cloud base was usually low, patchy fogs often formed below the cloud base. The visibility out of these fogs was, however, very good although the relative humidity in the boundary layer almost never dropped below 95 %. On can speculate that in this clean air, with a very low number concentration of CCN, fog formation requires a dynamic triggering and that the patchiness of the fog is thus a result of a dynamic feedback.

REFERENCES

Curry J. A. and A. H. Lynch 2002: Comparing Arctic Regional Climate Models. *EOS Trans. Amer. Geophys. Union.* , **83**, 87.

Garrett, T. J., L. F. Radke and P. V. Hobbs, 2002: Aerosol effects on cloud emissivity and surface longwave heating in the Arctic. J. Atmos. Sci., 59, 769 – 778.

Meehl, G. A., and coauthors, 2000: The Coupled Model Intercomparison Project (CMIP). *Bull. Am. Meteorol. Soc.*, **81**, 313-318.

Räisänen, J., 2001: CO2-induced climate change in the Arctic area in the CMIP2 experiments. SWECLIM News letter, **11**, 23 – 28.

Tjernström, M., 2004: The summer Arctic boundary layer during the Arctic Ocean Experiment 2001 (AOE-2001). *Bound.-Layer Meteorol.*, Submitted.

Tjernström, M., and coauthors, 2004: The Summertime Arctic Atmosphere: Meteorological measurements during the Arctic Ocean Experiment 2001 (AOE-2001). *Bull. Am. Meteorol. Soc.*, Accepted.

Tjernström, M., and coauthors, 2004: Modelling the Arctic boundary layer: An evaluation of six ARCMIP regional-scale models using data from the SHEBA project. *Bound.-Layer Meteorol.*, Submitted.

Walsh, J. E., W. M. Kattsov, W. L. Chapman, V. Govorkova and T. Pavlova, 2002: Comparison of Arctic climate by uncoupled and coupled global models. *J. Clim.*, **15**, 1429 – 1446.